Chapter-3

Effect of Sintering Temperature on Ion dynamics of $Na_{0.5}Bi_{0.5}TiO_{3-\delta}$

Pragati Singh, *Pardeep K. Jha, Priyanka A. Jha, Prabhakar Singh, "Influence of sintering temperature on ion dynamics of* $Na_{0.5}Bi_{0.5}TiO_{3-\delta}$*: Suitability as an electrolyte material for SOFC", International Journal of Hydrogen Energy, 2020,* 17006-17016.

CHAPTER 3: Effect of Sintering Temperature on Ion Dynamics of $Na_{0.5}Bi_{0.5}TiO_3$

3.1 Introduction

It has already been discussed in chapter 1, that $Na_{0.5}Bi_{0.5}TiO_3$ (NBT) is one of the promising electrolyte materials for SOFC. It crystallizes in rhombohedral structure at room temperature and undergoes a sequence of phase transitions with temperature[143]. In the intermediate temperature (IT-SOFC) range (500 ℃ -700 ℃), its crystal structure gets transformed to cubic phase at temperature around 520-540 ℃ [143]. There are several reports regarding the variation of processing parameters for NBT[144]–[146]. Their property got affected by the slight variation in stoichiometry. Moreover, the ion channels in the NBT system with the sintering temperature is not explored.

Hence, in this chapter, ion channels in NBT through ion dynamics and the applicability of different scaling mechanisms with the sintering temperature has been explored. As NBT is an ion-conducting material, it is vital to investigate the ion dynamics in order to comprehend its ionic conducting behaviour. Various groups and scientists have tried various ways to comprehend ion dynamics in a variety of systems, including glasses, polymers, semiconductors, nano-composites, and poly-crystals, and have succeeded in elucidating conduction mechanisms. Further, as the electrolyte samples are exposed to both the oxidizing and reducing atmosphere at the electrode end, it needs to be stable in both atmospheres. So, the stability of the sample is also checked in reducing the atmosphere.

3.2 Experimental Procedure

$Na_{0.5}Bi_{0.5}TiO_3$ ceramic samples were prepared by conventional solid-state reaction route. The high purity powders of Na_2CO_3 (Rankem 99.5%; India), Bi_2O_3 (SRL 99%; India), and TiO_2 (Merck 99% US) were mixed in stoichiometric proportions. A detailed synthesis and characterization procedure have already been discussed in chapter 2.

The phase formation was studied through Rigaku Miniflex desktopX-ray Diffractometer (XRD) with CuKα radiation (λ = 1.5405 Å) in the range 2θ ~ 20 - 70º with a step size of 0.01º. The diffraction patterns were refined by the Rietveld refinement method using FullProf suite software package. The microstructures of the sintered samples were studied using scanning electron microscopy (EVO - Scanning Electron Microscope MA15 / 18). The average grain size was calculated using the linear intercept method. The sintered pellets were then coated with platinum paste and cured at 700 ℃ for 30 min. The conductivity measurements were performed using the Wayne Kerr LCR meter (6500 P Series) as a function of frequency ranging from 20 Hz to 1 MHz at different temperatures starting from room temperature to 700 ℃ at the step of 5 ℃.

3.3 Results and Discussion

3.3.1 Structural Studies

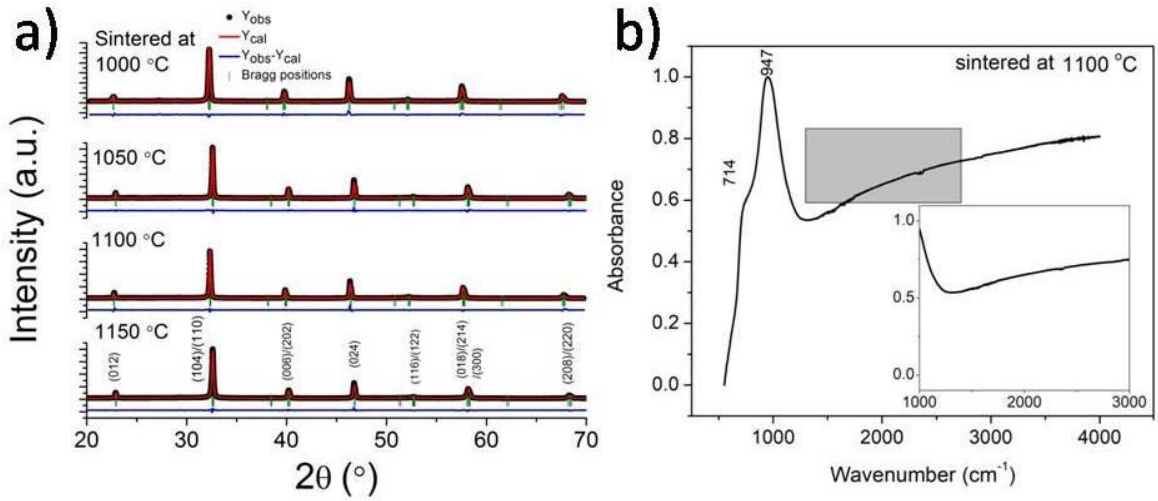

Figure 3.1: (a) Rietveld refinement of XRD pattern for different sintering temperatures **(b)** FTIR of the sample sintered at 1100 ℃

Figure 3.1(a) shows the Rietveld refinement of the samples sintered at different sintering temperatures, 1000 ℃, 1050 ℃, 1100 ℃ and 1150 ℃. The XRD data was refined using Full Prof Suite Package using R3c symmetry with Pseudo-Voigt peak profile and zero correction of the instrument. The lattice parameters, R-factors and the atomic positions obtained after refinement are listed in Table 3.1. It is observed that the R-factors for the refinement lie within the appreciable range. In order to identify the possibility of residual hydrocarbons during processing, FTIR of the pellet samples is recorded. Figure 3.1 (b) shows the FTIR pattern for the pellet sintered at 1100 ℃ (for instance). The peaks indexed at 714 cm^{-1} and 947 cm^{-1} are the characteristic features of NBT[145]. However, we were unable to observe any significant feature of any hydrocarbon, e.g., PVA, ethanol, acetone etc., used

during the processing of these samples. Since PVA has very low boiling/melting points, i.e. (230 ℃ or 200 ℃, respectively) and its burn out profile indicates that its gaseous products gets driven off and do not remain inside the sample after sintering[147].

Table 3.1: Atomic positions and R-factors obtained after refinement for the $Na_{0.5}Bi_{0.5}TiO_3$ samples sintered at different temperature

Sintering Temperature	Lattice parameters (Å)	Atoms	Position coordinates			R-factors	
			x	y	z	Bragg R-factor	R_f factor
1000 ℃	a= b=5.4855 c =13.4766	Na	0	0	0.25012	2.93	3.07
		Bi	0	0	0.25015		
		Ti	0	0	0.00479		
		O	-0.16673	0.20048	0.11543		
1050 ℃	a = b =5.5373 c =13.5451	Na	0	0	0.59166	3.83	2.95
		Bi	0	0	0.59166		
		Ti	0	0	0.34364		
		O	-0.16090	0.18499	0.30225		
1100 ℃	a = b =5.4899 c =13.4649	Na	0	0	0.24488	3.64	2.42
		Bi	0	0	0.24488		
		Ti	0	0	0.00209		
		O	-0.16413	0.29955	0.05092		
1150 ℃	a = b =5.5422 c =13.6287	Na	0	0	0.39744	4.37	2.39
		Bi	0	0	0.39744		
		Ti	0	0	0.15519		
		O	-0.14363	0.21041	0.02651		

3.3.2 AC Conductivity Formalism

Figure 3.2 depicts the variation of log σ vs log ν for the samples synthesized under different sintering temperatures. The electrical behaviour of the studied samples is well described using modified Jonscher Power law given by[148]

$$\sigma_{ac} = \sigma_o + A\nu^n = \sigma_{dc}\left[1 + \left(\frac{\nu}{\nu_h}\right)^n\right] \quad (3.1)$$

where, σ_o is the frequency independent conductivity, A is constant, ν is the frequency of the applied electric field and ν_h is the crossover frequency and n represents the degree of interaction between the mobile ions with the lattice. Here, the symbol represents the experimental data, and the solid line represents the power line fitted curve using eqn. 3.1. It is observed in Fig. 3.2 that there is a plateau at low temperature followed by an increase in conductivity at higher frequency. It is also observed in Fig. 3.2 that there are parallel isotherms in the sample sintered at 1000 ℃ in comparison to the merging of the isotherms at higher frequencies in the samples sintered at temperature >1000 ℃ (shown in gray region). Usually, in the conductivity isotherms, there is onset in the value of conductivity after the hopping frequency[149][150]. The DC conductivity represents the random hopping motion (successful hops) of the mobile charge carriers, and the dispersive regime represents correlated forward-backward motion (the unsuccessful hops) of the mobile charge carriers. In fact, the increase in conductivity with the increase in sintering temperature represents an increase in the hopping rate of the mobile charge carriers[151]. This fact is also reflected by the ratio ($\frac{\sigma_{dc}}{\nu_h}$) which is observed to decrease with the increase in sintering temperature. The ($\frac{\sigma_{dc}}{\nu_h}$) factor decreases due to increase in the hopping rate. To analyse further, the parameters derived after fitting the data are dc conductivity (σ_{dc}), hopping frequency (ν_h) and exponent (n) are studied.

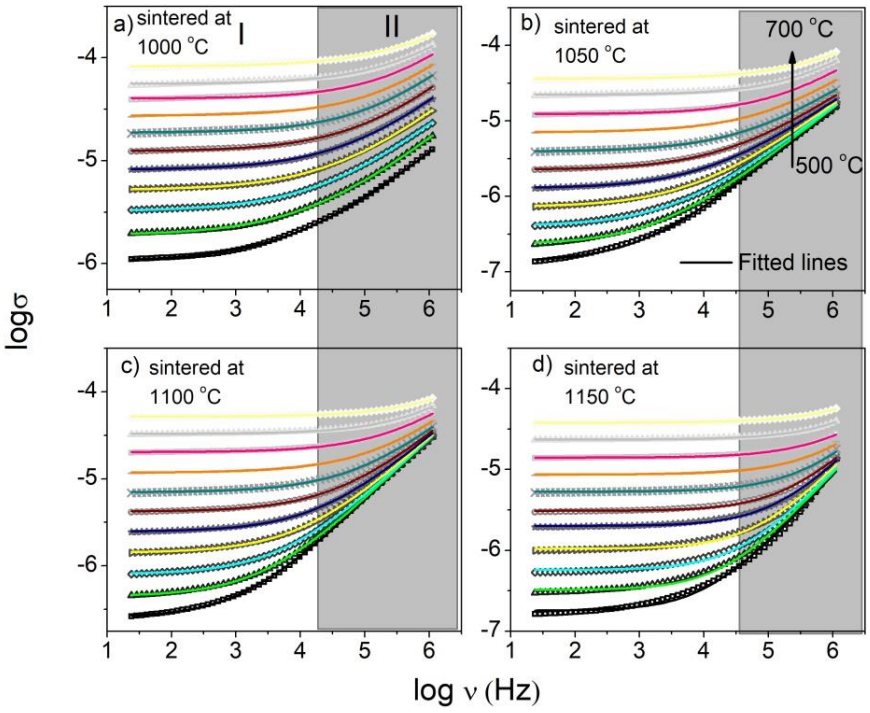

Figure 3.2: Depicts the variation of log σ vs log ν from 500 ℃ to 700 ℃ at the step of 20 ℃ for the samples synthesized under different sintering temperatures **(a)** 1000 ℃ **(b)** 1050 ℃ **(c)** 1100 ℃ **(d)** 1150 ℃

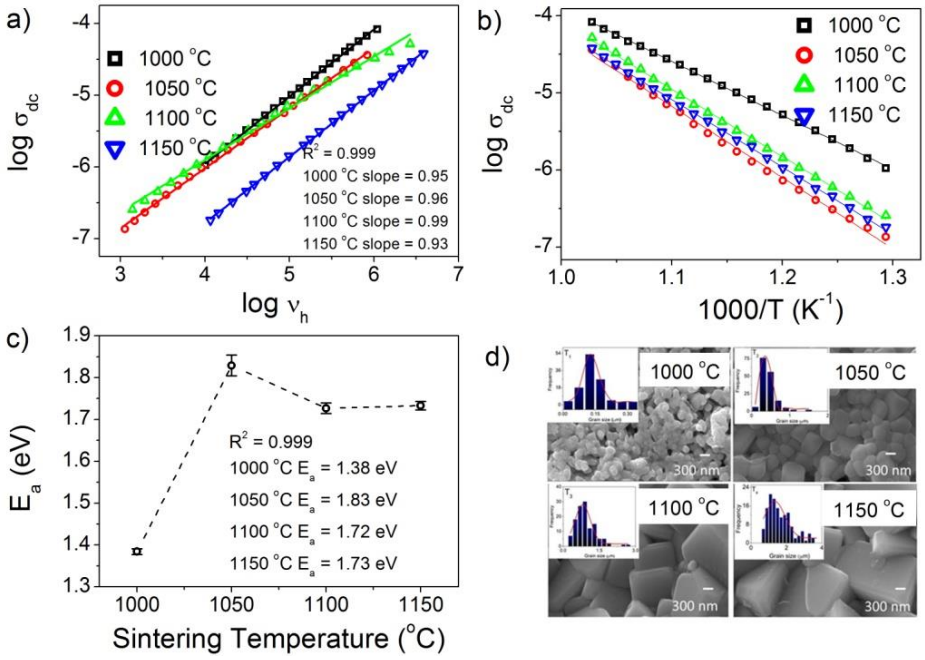

Figure 3.3: (a) Variation of log σ_{dc} vs log ν_h **(b)** Arrhenius plot for estimation of activation energy for the samples synthesized under different sintering temperatures, **(c)** Variation of E_a with sintering temperature and **(d)** SEM micrographs of the samples sintered at different sintering temperatures and respective insets shows their grain size histograms

Figure 3.3 (a) depicts the variation of log σ_{dc} vs log ν_h for the studied samples, and the slope obtained is nearly unity. This indicates that dc conductivity and hopping frequency are proportional to each other; hence, conductivity is governed through hopping[152][153]. The activation energy (E_a) is estimated for the studied samples using the Arrhenius equation $\sigma_{dc}T = \sigma_0 \exp\left(\frac{-E_a}{KT}\right)$ (shown in Fig. 3.3(b)) and plotted in Fig.3.3(c). It is observed that the activation energy for the sample sintered at temperature > 1000 ^oC has significantly increased. It may be the reason why dc conductivity is smaller for the sample sintered at higher temperature as higher cation vacancy increases activation and decreases conductivity[154]. It is recently reported that E_a required for the migration of Na^+ ion lies in between 2 eV and 4 eV, Bi^{3+} requires 5eV and 9 eV, and for the migration of oxide ions from NaO^- layer to TiO_2 layer, E_a is in between 1.82eV and 0.93eV[154]. In addition, the possible ordering of Bi^{3+}/Na^+ generates different local chemical environments for oxygen vacancies[155]. Thus, this activation energy of the range of 1.5-1.8eV suggests the migration of oxide ions from NaO^- layer to TiO_2 layer, but the difference of 0.5eV with the sintering temperature may be accounted in terms of microstructural variation (see Fig. 3.3 (d)). The activation energy for the sample sintered at temperature $\geq$ 1100 ℃ is nearly the same for 1000 ℃ and 1150 ℃. The difference in activation energy from 1000 ℃ to 1150 ℃ can be coupled with microstructural grain shape change from spherical to cubic grains along with the increase in the grain size from 0.1 μm to 1.5 μm with the increase in the sintering temperature from 1000 ℃ to 1150 ℃ and nearly same activation energy has observed for the stable cubic grains[154]. The conductivity of polycrystalline ceramic samples prominently depends on the shape, size and orientation of the grains and grain boundaries. The SEM microstructure (Fig. .3.3 (d)) reveals that for the sample sintered at 1000 ℃, the grains are not well developed showing large grain-grain

boundary interface area. At 1050 ℃, the grains start growing and shows grains having spherical as well as cubic shapes. The grains further grow at 1100 ℃ in cubic form, and finally, the grain growth stabilises in terms of large cubic grains at the sintering temperatures 1150 ℃ with lesser grain-grain boundary interface area. The charges available at the interfaces are contributing significantly to the conduction process and conductivity is proportional to the interface area. The activation energy also predicted the same trend as explained above. The exponent is plotted versus temperature for the sample synthesized under different sintering temperatures.

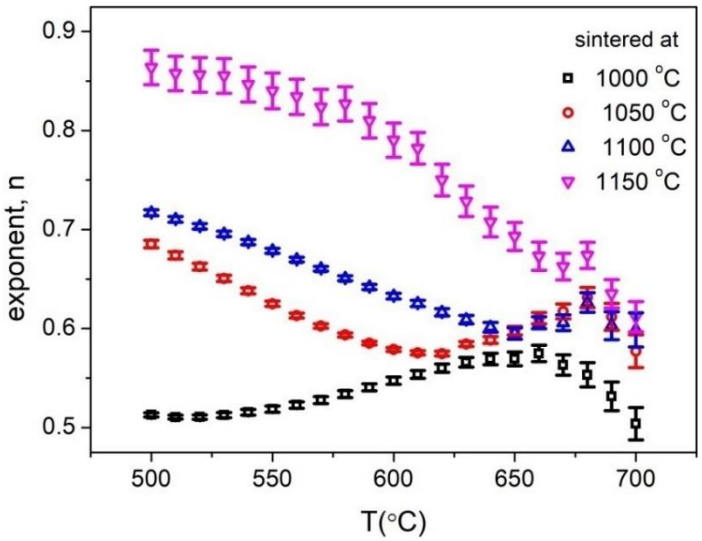

Figure 3.4: Variation of 'n' with temperature for the samples synthesized under different sintering temperatures

Figure 3.4 shows the variation of 'n' with temperature for the studied samples. It is observed that for the sample sintered at 1000 ℃, exponent increases with the increase in temperature. Whereas, for the samples sintered ≥ 1050 ℃, exponent is observed to decrease with the increase in temperature as shown in Fig. 3.4. The Almond-West formalism is used to evaluate the carrier concentration factor N, i.e. proportional to carrier concentration given by $N = \frac{\sigma_{dc}}{\nu_h}$, where σ_{dc} is the DC conductivity and ν_h is the hopping frequency[133]. Figure 3.5

depicts the variation of charge carrier concentration factor for the studied samples. It is observed that for the samples sintered at 1100 ℃ and 1150 ℃, the value of charge carrier concentration factor considerably reduces with the increase in temperature. From the variation of exponent and charge carrier concentration factor indicates that the sample sintered at 1000 ℃ is less ionic in comparison to the sample sintered at 1150 ℃. Also, the sample sintered at 1000 ℃ shows the formation of small polarons and the samples sintered at 1150 ℃ shows the feasibility of overlapping large polaron tunnelling mechanism[156].

The decrease in the dc conduction (see Fig.3.2) for samples sintered at temperature > 1000 °C may be interpreted in terms of the microstructural variation (see Fig. 3.3(d)). It is observed that for the sample sintered at 1000 °C, the grains are spherical and small, while for other samples with sintering temperature >1000 °C, the grains are increasing in size with the formation of cubes and are well connected with each other. It appears this morphological change from sphere to cube with the increase in sintering temperature has altered the physical property as activation energy is significantly different for sample sintered at 1000 °C as compared to other samples. In addition, the merging at high frequency up to 600 °C is observed for the well-connected cubic grains. Additionally, the increase in the grain size with sintering temperature also affects the charge/ion dynamics (as seen above in the variation of exponent and charge carrier concentration). The mechanism behind these observations can be understood in terms of microstructure variation. The well-developed micro-structure with large grains leads to the lesser volume of grain boundaries. Simultaneously, the charge carriers at the interface reduce, affecting the grain-grain boundary contact area. Thus, due to the decrease in charge carrier concentration at the grain-grain boundary interfaces, the conductivity reduces[157].

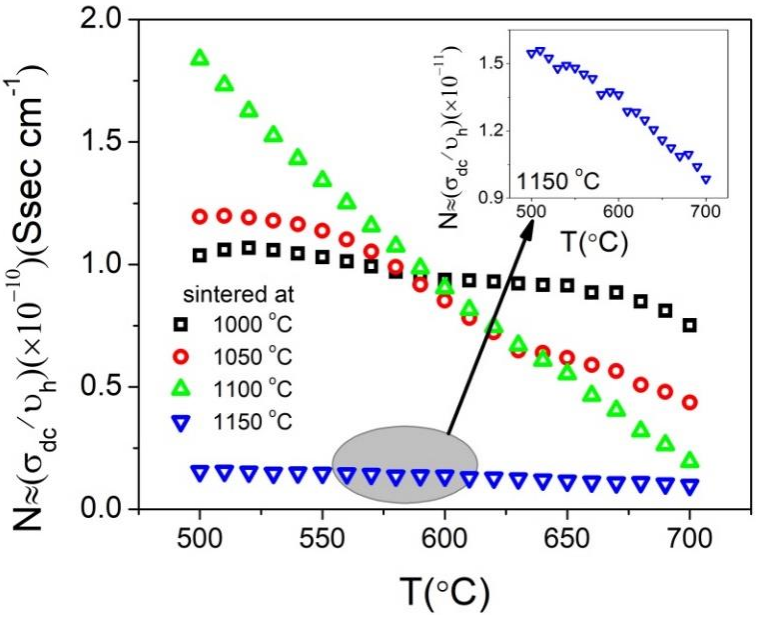

Figure 3.5: Variation of charge carrier concentration factor 'N' with temperature for the samples synthesized under different sintering temperatures

3.3.3 Scaling Mechanism

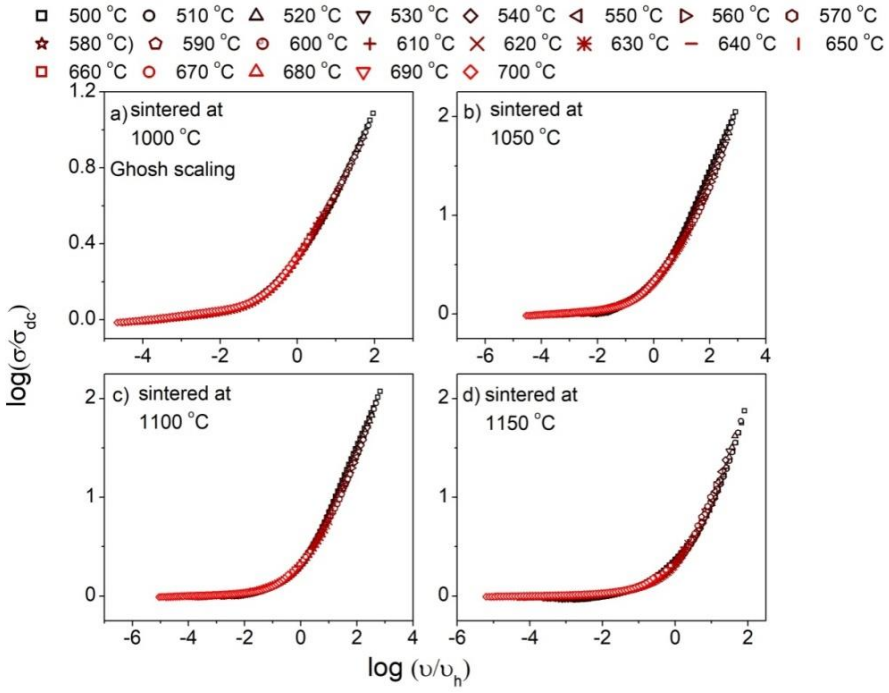

Figure 3.6: Ghosh scaling for the samples synthesized under different sintering temperatures

In order to understand the structure disorder and randomness (Random free energy barrier model)[152] various scaling mechanisms have been employed. For this, Ghosh scaling[158], Summerfield[159] and Modulus scaling have been applied. Figure 3.6 depicts the Ghosh scaling for the studied samples. The conductivity isotherms are very well defined using Ghosh scaling in the studied samples, i.e. they follow the time-temperature superposition principle (TTSP). It indicates the quantitative increase in charge carriers rather than their nature. Figure 3.7 indicates the Summerfield scaling for all the studied samples. When Summerfield scaling has been applied, it is observed that it is well resolved for the sample sintered at 1150 ℃ in comparison to the Summerfield scaling applied in case of the sample sintered at 1000 ℃.

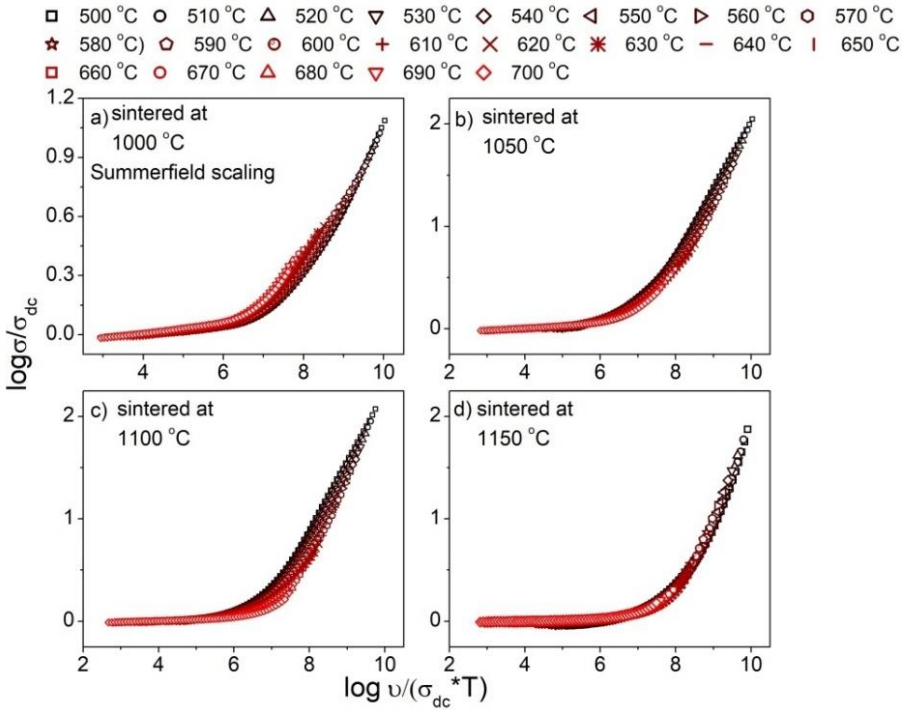

Figure 3.7: Summerfield scaling for the samples synthesized under different sintering temperatures

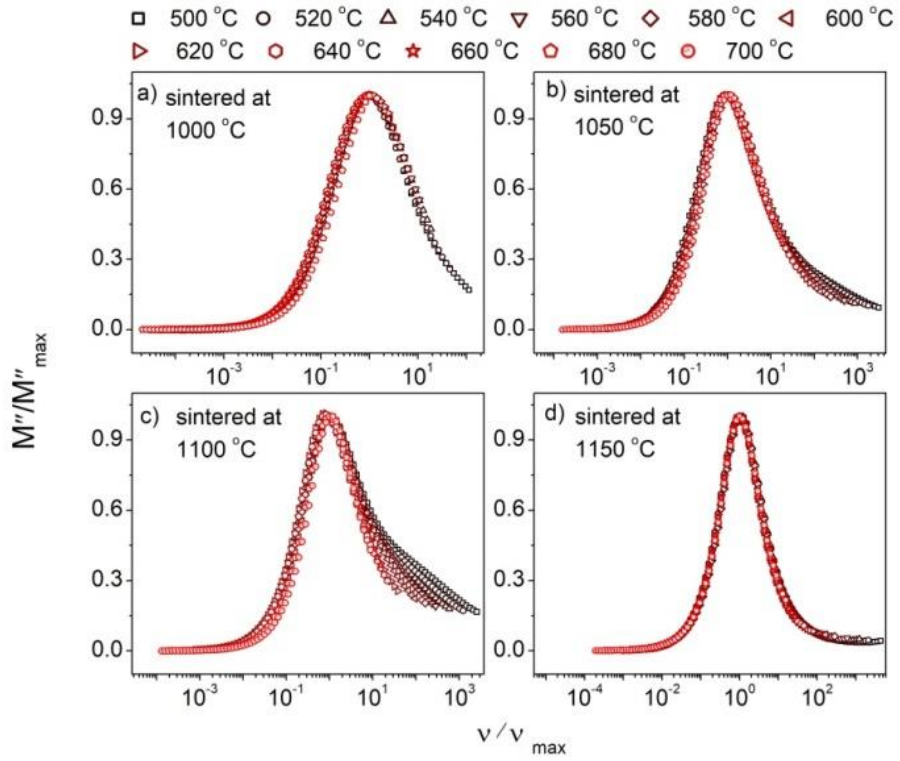

Figure 3.8: Modulus scaling (M"/M"$_{max}$vs ν/ν$_{max}$) with the variation of sintering temperature **(a)** 1000 ℃ **(b)** 1050 ℃ **(c)** 1100 ℃ **(d)** 1150 ℃

Figure 3.8 shows the modulus scaling (M"/M"$_{max}$ vs ν/ν$_{max}$) with the variation of sintering temperature. It is observed that modulus scaling followed in the sample sintered at 1150 ℃, indicating that the ion dynamics is temperature independent. Hence, in the sample sintered at 1150 ℃ followed Ghosh scaling, Summerfield and Modulus scaling in comparison to other samples. The Summerfield scaling indicates the alterations in Bi-Ti channels with the sintering temperature[159]. To understand the alterations in Bi-Ti channels, the Bi-Ti distance (Fig. 3.9) are obtained from Diamond software using cif files obtained from Rietveld refinement of the XRD (discussed earlier). The structure thus obtained from Diamond software is shown in Fig. 3.9 (inset). As Bi-Ti distance (shown in Fig. 3.9) is greater than 2.8Å ($r_{O^{2-}}$)[160] ion, but it is lower for the sample sintered at 1150 ºC in comparison to the other sintered samples.

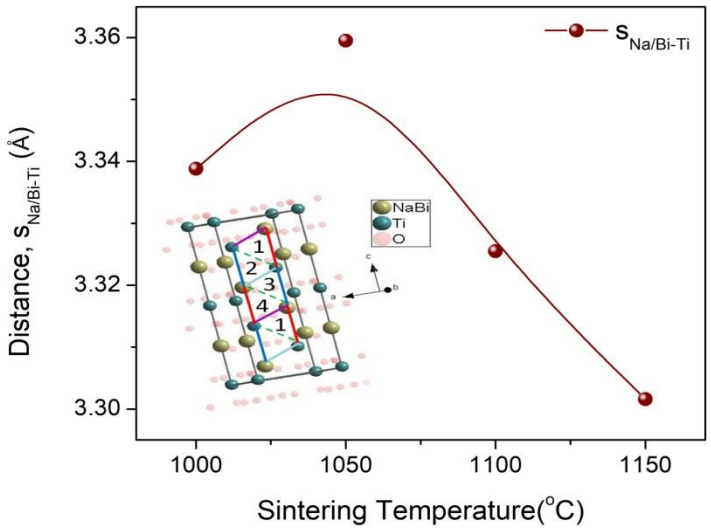

Figure 3.9: Variation of Na/Bi-Ti bond with the sintering temperature (inset) structure of NBT from Diamond

3.3.4 Differential Impedance Analysis

As observed earlier, the conduction is taking place through the diffusion of ions in the lattice. For the distribution of charge carriers, the differential impedance analysis technique is used. The values of K are calculated from log |Z| vs log ν (shown in Fig. 3.10) in the temperature range of 500 ℃ to 700 ℃ for the studied samples as per the relation $|Z|_{adj} = f^{-K}$[161][162]. Figure 3.11 shows the value of K obtained from the slope of Fig. 3.10 in the high frequency regime. The value of K for the sample sintered at 1000 ℃ is continuously decreasing with temperature and reaches the minimum value of 0.4, showing the charge carriers are moving with the hindrance in the matrix[163]. While for the samples sintered at higher temperatures, K value is nearly constant up to 650 ℃ and thereafter decreases with the further increase in temperature. This shows that the charge carriers are moving without any hindrance in the samples sintered at sintering temperatures greater than 1000 ℃.

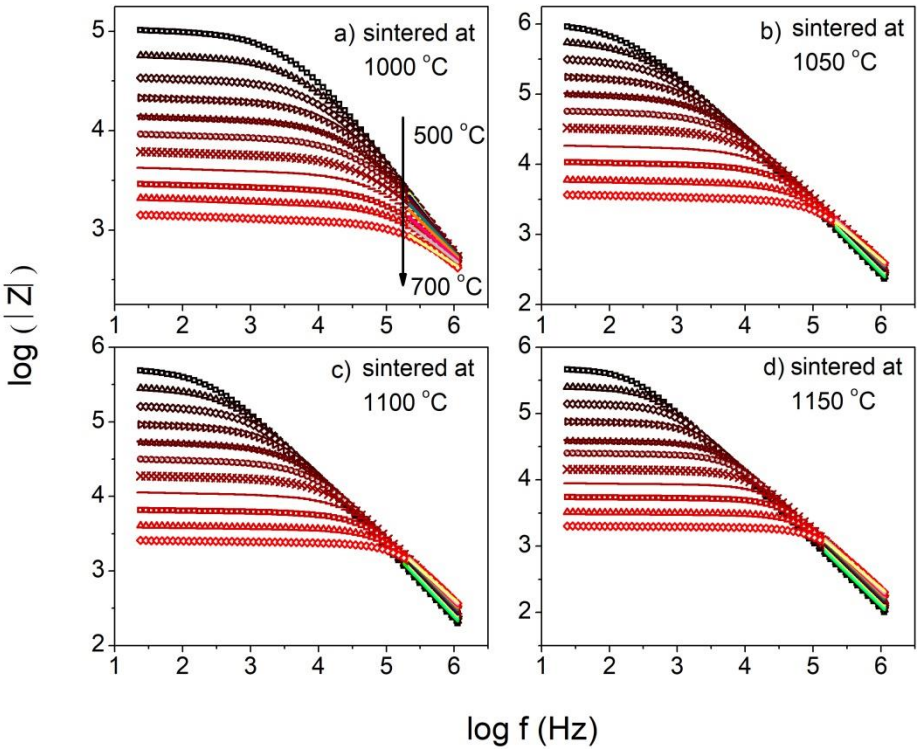

Figure 3.10: Estimation of K using relation $|Z|_{adj} = f^{-K}$ from log |Z| vs log ν for all the studied samples

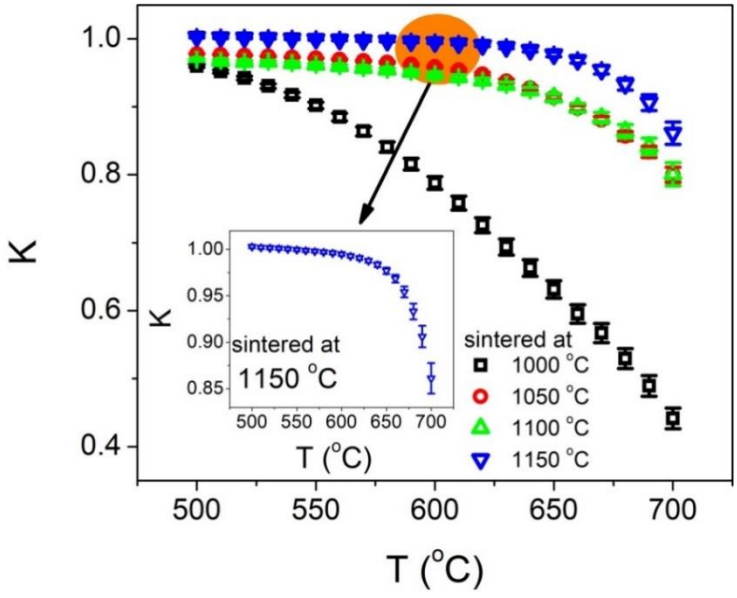

Figure 3.11: Variation of K with temperature ranging from 500 ℃ to 700 ℃ for all the studied samples

3.3.5 Correlation of structural and electrical behaviour

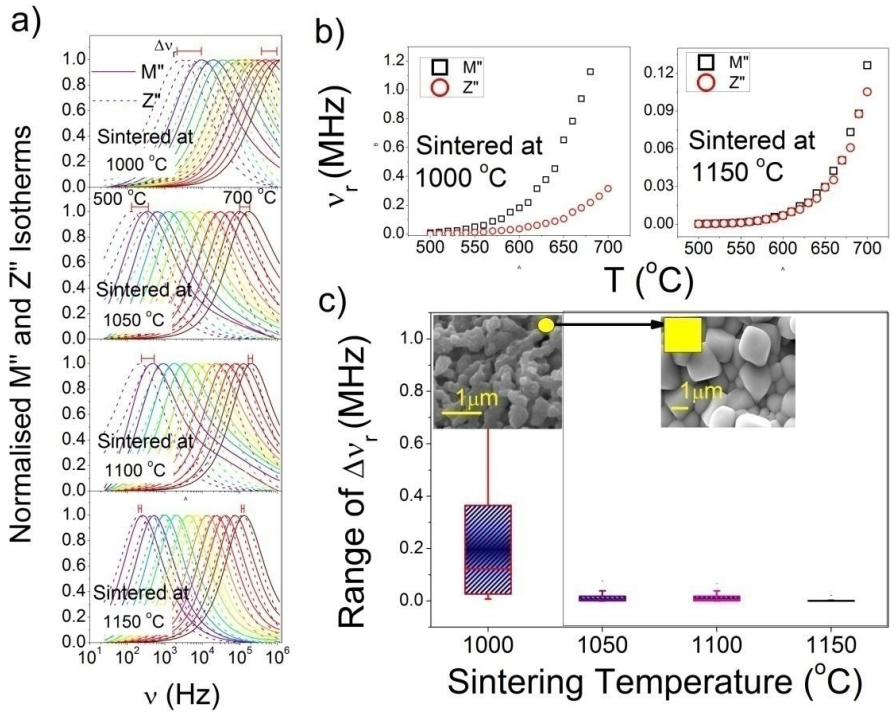

Figure 3.12: (a) Normalized M" and Z" isotherms with frequency in the temperature range of 500 ℃ to 700 ℃ with the variation of sintering temperature **(b)** Variation of relaxation hopping frequency with temperature for the samples sintered at 1000 ℃ and 1150 ℃**(c)** Range of $\Delta\nu_r$ for all the studied samples

For the illustration of the observation of small polaron in the sample sintered at 1000 ℃ and large polaron in the temperature>1000 ℃, normalized M" and Z" isotherms are plotted with frequency in the temperature range of 500 ℃ to 700 ℃ with the variation of sintering temperature (Fig. 3.12(a)). The difference between hopping frequency $\Delta\nu_r$ (i.e., the frequency corresponding to the maxima of Z" and M") is represented by the horizontal bar for isotherms corresponding to temperature 500 ℃ and 700 ℃. It is observed that for both the isotherms, i.e., $\Delta\nu_r$ at 500 ℃ and 700 ℃ reduces with the increase in sintering temperature and nearly overlapped in the sample sintered at 1150 ℃. However, due to non-linear variation of hopping frequency with temperature, the horizontal length of $\Delta\nu_r$ for two isotherms cannot be compared.

In order to reveal the temperature dependent variation of hopping frequency within the sample, Fig 3.12(b) is plotted. Fig. 3.12(b) shows the variation of relaxation hopping frequency with temperature for the samples sintered at 1000 ℃ and 1150 ℃. It is observed that the relaxation hopping frequency obtained from M'' and Z'' are separating widely in the sample sintered at 1000 ℃, whereas the relaxation hopping frequency obtained from M'' and Z'' are merging in the sample sintered at 1150 ℃. Figure 3.12(c) depicts the range of $\Delta\nu_r$ for all the studied samples. It is observed that the range of $\Delta\nu_r$ is wide for the temperature range studied in case of sample sintered at 1000 ℃, hinting the short range hopping of charge carriers in this porous sample (1000 ℃). With increase in the sintering temperature, $\Delta\nu_r$ is reducing and finally merging for the sample sintered at 1150 ℃, indicating the possibility of long range hopping of charge carriers in dense samples (>1000 ℃)[164].

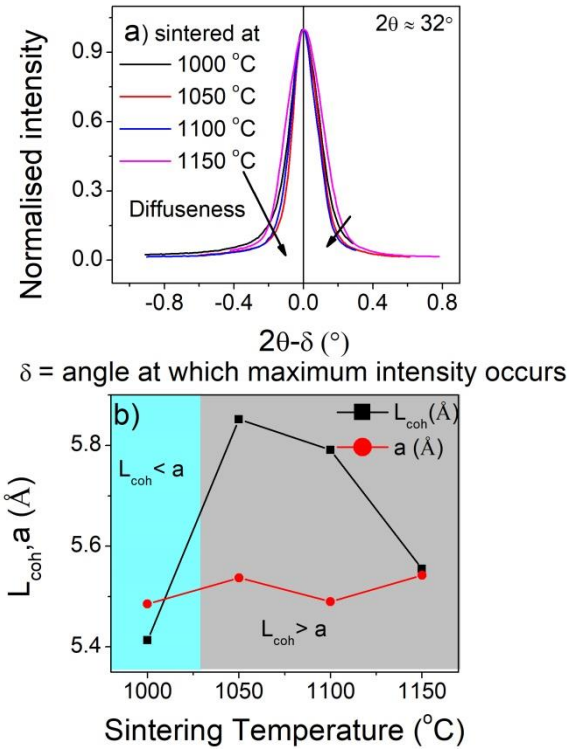

Figure 3.13: (a) Plot of XRD intensity of peak (2θ~32°) vs 2θ-δ (°) where δ is the angle at which maxima occurs showing diffuseness of XRD peak with the sintering temperature, **(b)** Variation of coherence length, L_{coh} and lattice constant, a with the sintering temperature

For the further verification of polarons, structural data is used. Figure 3.13 (a) shows the plot of intensity of XRD peak corresponding to 2θ ~32° vs 2θ-δ (°) where δ is the angle at which maximum intensity occurs. It is observed that peaks are becoming more diffusive with the increase in sintering temperature showing the polaron formation[164][165]. Figure 3.13 (b) illustrates the variation of room temperature coherence length, L_{coh}, and lattice constant, a, with the sintering temperature. It is observed that L_{coh}< a for the sample sintered at 1000 ℃, whereas L_{coh}> a for the samples sintered at sintering temperature higher than 1000 ℃[166]. This indicates the formation of small polarons at 1000 ℃ and large polarons at 1150 ℃ at room temperature. As the sample undergoes a tetragonal to cubic phase transition at 520 ℃ and hence, the lattice parameter will change and in any case coherence length will be greater than the lattice constant.

3.3.6 Stability under reducing atmosphere

For SOFC, electrolyte material which is ionic in nature, one should know how the electrolyte materials behave in reducing conditions as it has an interface with the anode that is operated in reducing atmosphere. For this, we placed the sample in propan-2-ol (dielectric constant ~ 20 at room temperature) for 2 days. We compared the XRD pattern and electrical features at room temperature of the NBT sample and the sample dipped in propan-2-ol. Figure 3.14 shows the X-ray diffractograms of the NBT sample and the sample dipped in propan-2-ol (C_3H_7OH) for two days. It is observed that some more peaks corresponding to $C_6H_9BiO_6$ (PCPDF No. 147026) have appeared with the reaction of NBT with propan-2-ol in addition with the left shifting of the XRD peaks. Further, the inset of this figure represents (i) log σ vs log ν for the NBT sample and sample dipped in propan-2-ol (ii) Modulus Nyquist plots at room temperature for the NBT sample and sample dipped in propan-2-ol (iii) Gray highlighted region of inset (ii) showing modulus Nyquist plots of pure NBT sample at room temperature. It is observed that lattice got shrink as well as crystallite size reduces which clearly hints that grains get separated with the enlargement of grain boundary. The modulus spectroscopy clearly supports the fact. Also, conductivity gets reduced by one order of magnitude. Thus, the sample is expected to degrade in H_2 atmosphere as well.

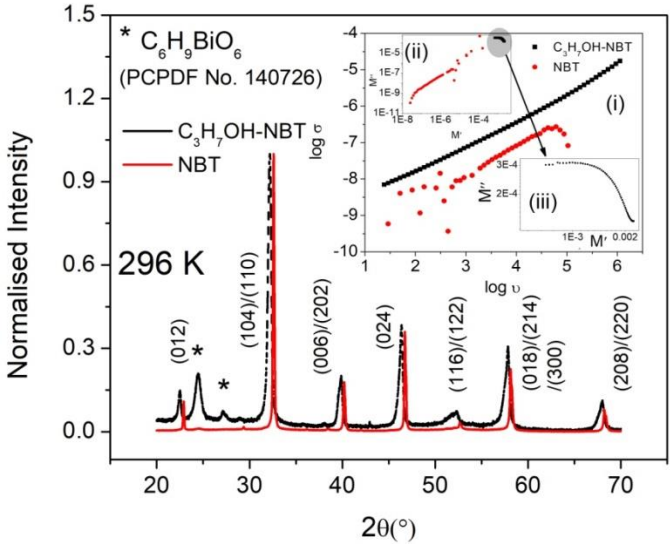

Figure 3.14: X-ray diffractograms of the NBT sample and the sample dipped in propan-2-ol (C_3H_7OH) for two days **(i)** log σ vs log ν for the NBT sample and sample dipped in propan-2-ol**(ii)** Modulus Nyquist plots at room temperature for the NBT sample and sample dipped in propan-2-ol (iii) Gray highlighted region of inset **(ii)** showing modulus Nyquist plots of pure NBT sample at room temperature

3.4 Conclusion

The conduction mechanism observed here suggests the migration of oxide ions from NaO^- layer to TiO_2 layer with the activation energy of the range of 1.5 - 1.8 eV. The observed difference of E_a = 1.3 eV to 1.8 eV with the sintering temperature may be accounted in terms of microstructural variation. With the increase in the sintering temperature the grain size is increasing, but the other significant variation is in terms of shape of grains. However, this requires a more focussed and detailed discussion. In addition to it, long range oxide ion diffusion is occurring with the formation of large polarons at 1150 ℃. It can also be interpreted that the sample sintered at 1150 ℃ is more ionic as compared to the sample sintered at 1000 ℃. However, the sample is observed to degrade in reducing atmosphere.